Chemical Science

ROYAL SOCIETY OF CHEMISTRY

EDGE ARTICLE

View Article Online
View Journal | View Issue

Cite this: *Chem. Sci.*, 2025, **16**, 18223

All publication charges for this article have been paid for by the Royal Society of Chemistry

Carboxylato-prism[6]arene as a supramolecular catalyst in water: exploiting its deep hydrophobic cavity for green oxidation of aromatic amines

Rocco Del Regno, [a] Giuseppa Campanile, [a] Placido Neri, [a] Carmen Talotta, [a] Antonio Rescifina, *[b] Carmelo Sgarlata, *[c] Giuseppina D. G. Santonoceta,[c] Carmine Gaeta [a] and Margherita De Rosa *[a]

Received 30th April 2025
Accepted 28th August 2025

DOI: 10.1039/d5sc03155a

rsc.li/chemical-science

The carboxylato-prism[6]arene acts as an efficient catalyst for the oxidation of aromatic amines in water, utilizing hydrogen peroxide (H_2O_2) as a green oxidant. The findings indicate that forming supramolecular endo-cavity complexes between aniline derivatives and the prism[6]arene is essential for catalytic activity. Calorimetric investigations demonstrate that this complex formation is primarily driven by entropic factors associated with expulsing frustrated water molecules from the deep hydrophobic cavity of the prism[6]arene. *In silico* studies further confirm the presence of these water molecules within the cavity and their subsequent release upon the introduction of aromatic amines. Additionally, a computational approach was employed to elucidate the initial oxidation steps of aniline within the prism[6]arene cavity. This encapsulation process significantly lowers the activation free energy by 34.94 kJ mol^{-1}, thereby enhancing reactivity through hydrogen bonding and solvent effects. The computational results closely align with experimental data, underscoring the critical role of host–guest interactions within the deep cavity of the prism[6]arene in facilitating the oxidation process.

Introduction

Natural enzymes are known for their outstanding catalytic efficiency, selectivity, and specificity.[1–3] This inherent ability has generated significant interest in developing artificial enzyme mimetics[4,5] designed to replicate these properties and facilitate various chemical transformations. As a result, many artificial enzymes have been engineered utilizing various supramolecular frameworks.[5–7] These scaffolds range from macrocycles featuring hydrophobic cavities, such as cyclodextrins,[8] calixarenes,[9] cucurbiturils,[10] resorcinarenes,[11] and pillararenes,[12] to self-assembled nanoscaled architectures[13–17] and beyond. Many of these supramolecular scaffolds have been utilized as nanoreactors for catalytic applications, particularly in aqueous environments, underscoring their potential to enhance reaction efficiency and promote environmentally benign catalysis.[7]

Aromatic nitro compounds are versatile intermediates in organic synthesis and the fine chemical industry.[18] They have been extensively utilized as explosives and precursors for azo dyes.[19] More recently, they have demonstrated considerable potential in various fields, including pharmaceuticals,[20] materials for molecular electronics,[21] and fragrances.[22]

Nitroarenes are conventionally synthesized through the direct nitration of aromatic compounds using nitric acid or a mixture of nitric and sulfuric acids. These methods often depend on costly and less sustainable organic solvents,[23,24] are sensitive to water and produce significant waste. In response to these limitations, recent efforts have focused on developing greener synthetic routes using alternative protocols.[25–27] One particularly attractive approach involves the direct oxidation of readily available and inexpensive aromatic amines into nitroarenes, offering an efficient and environmentally friendly alternative.[23–27] To this end, several methods have been reported, utilizing various oxidizing agents and catalysts to achieve eco-friendly processes.[25–27] Nonetheless, many of these approaches are hindered by the use of costly catalytic systems, prolonged reaction times, the generation of significant waste, and a lack of selectivity, often resulting in a mixture of various oxidation products.[25–27] Therefore, developing mild, sustainable, and efficient oxidation processes is highly desirable.[23–27] Supramolecular approaches offer a promising route to environmentally benign oxidation of aromatic amines.[28,29] Several studies[28,29] have reported the successful oxidation of anilines to nitro compounds using hydrogen peroxide, facilitated by the formation of supramolecular complexes such as aniline@-cyclodextrin. The hydrophobic cavity of the cyclodextrin host

[a]*Laboratory of Supramolecular Chemistry, Department of Chemistry and Biology "A. Zambelli", University of Salerno, Via Giovanni Paolo II, Fisciano (SA), I-84084, Italy. E-mail: maderosa@unisa.it*

[b]*Department of Drug and Health Sciences, University of Catania, V.le A. Doria 6, 95125 Catania, Italy. E-mail: antonio.rescifina@unict.it*

[c]*Department of Chemical Sciences, University of Catania, V.le A. Doria 6, 95125 Catania, Italy. E-mail: sgarlata@unict.it*

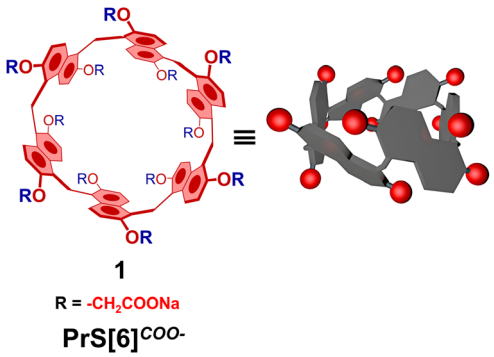

Fig. 1 Chemical structure of carboxylato-prism[6]arene PrS[6]$^{COO-}$ investigated in this work as a nanocontainer for the green oxidation of aniline derivatives.

enhances the local concentration of the aniline substrate in water, promoting reaction through a mechanism analogous to enzyme–substrate interactions and improving reaction rates.

Our research group has recently introduced prism[n]arenes,[30–34] a novel class of macrocyclic compounds composed of 1,5-methylene-bridged naphthalene units (Fig. 1). The peculiar structure and conformation of these compounds make them promising supramolecular catalysts, featuring a deep, π-electron-rich aromatic cavity that is well-suited for binding various organic reactants.

Furthermore, the two oxygenated rims of prism[n]arenes can be easily functionalized[32] with catalytically relevant groups, providing additional opportunities to enhance their catalytic performance.

For instance, we successfully synthesized carboxylato-prismarenes[32] by appending anionic carboxylate functions to the rims of the prismarenes, resulting in water-soluble hosts capable of encapsulating neutral organic molecules within their hydrophobic cavities.[34] Building upon this,[34] we now report a mild and selective catalytic method for oxidizing arylamines to nitro derivatives. This approach utilizes carboxylato-prism[6]arene to enhance the reactivity of anilines with hydrogen peroxide (H_2O_2), a green and inexpensive oxidant.

Our method offers significant advantages, including a streamlined protocol, high atom economy, and the use of water as the sole solvent and byproduct, which significantly reduces environmental impact.

Results and discussion

Aniline **2a** (Scheme 1) was selected as the model substrate for our initial studies. When the reaction was conducted in the presence of 1 equivalent of carboxylato-prism[6]arene **PrS[6]$^{COO-}$**,[33] and 2 mL of hydrogen peroxide (50 wt% solution in water) at 60 °C, the nitro derivative **3a** was obtained in high yield (92%) after only 2 hours (Table 1, entry 2). No evidence of side oxidation products was detected in the reaction mixture. Conversely, a control experiment conducted under identical conditions but without the presence of **PrS[6]$^{COO-}$** showed a markedly lower yield (10%) of **3a**, accompanied by the formation of a complex mixture of various *N*-oxidation products (Table 1, entry 1 and SI). Furthermore, performing the reaction in the presence of *N*,*N*,*N*′,*N*′-tetramethylpiperazonium diiodide salt, which serves as a competitive guest with a strong affinity

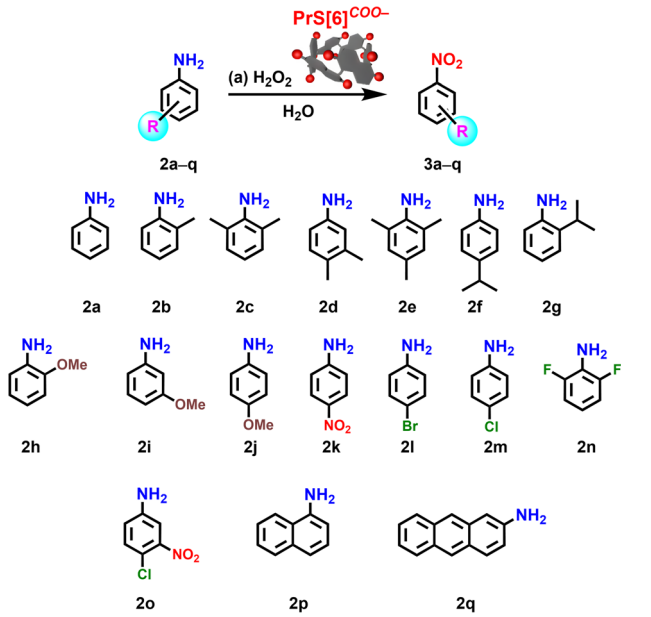

Scheme 1 Oxidation of aniline derivatives **2a–q** in the presence of carboxylato-prism[6]arene PrS[6]$^{COO-}$ as nano-container. (a) Conditions reported in Tables 1 and 2.

Table 1 Optimization of the reaction conditions for the oxidation of aniline **2a** in the presence of PrS[6]$^{COO-}$ [a]

Entry	PrS[6]$^{COO-}$ (equiv.)	H_2O_2, mL (equiv.)	T (°C)	t (h)	Yield[b] (%)
1	—	2 (350)	60	2	10[c]
2	1.0	2 (350)	60	2	92
3[d]	1.0	2 (350)	60	2	—
4	0.50	2 (350)	60	2	74
5	0.30	2 (350)	60	2	74
6	0.15	2 (350)	60	2	74
7	0.05	2 (350)	60	2	36
8	0.15	2 (350)	60	4	75
9	0.15	2 (350)	60	1	63
10	0.15	2 (350)	40	2	36
11	0.15	2 (350)	25	4	40
12	0.15	2 (350)	25	15	65
13[e]	0.50	1 (175)[f]	60	2	71
14[e]	0.50	0.5 (87.5)[e]	60	2	23
15[e]	0.50	0.5 (87.5)[e]	60	7	56
16[e]	0.50	0.25 (43.8)[e]	60	2	13
17[e]	0.30	0.5 (87.5)[e]	60	7	4

[a] Reactions were performed on a 0.1 mmol scale of aniline **2a** with 50% aqueous H_2O_2. [b] Yields determined by ^{1}H NMR analysis of the crude reaction mixture using as internal standard 1,1,2-trichloroethane. [c] The crude reaction mixture contains a significant amount of starting material **2a** and various oxidation products (Fig. S4). [d] The reaction was performed in the presence of *N*,*N*,*N*′,*N*′-tetramethylpiperazonium diiodide salt (1 equiv.). [e] Phosphate buffer (68 mM, pH 7.6) was added to the reaction mixture: 1 mL for entry 13, 1.5 mL for entries 14–15, 17, and 1.75 mL for entry 16. [f] ref. 36.

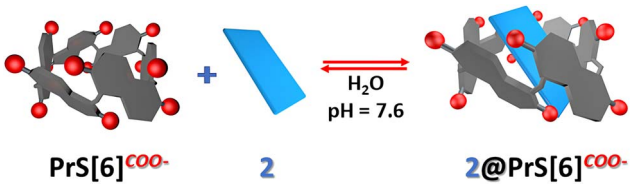

Fig. 2 Cartoon representation of the complexation equilibrium of prism[6]arene **PrS[6]**$^{COO-}$ with aniline derivatives at 25 °C in a buffered aqueous solution (pH 7.6).

for **PrS[6]**$^{COO-}$,[32] yielded no evidence for the formation of the nitro derivative **3a** (Table 1, entry 3). These preliminary findings provide the first indication that **PrS[6]**$^{COO-}$ can indeed facilitate the reaction by activating hydrogen peroxide. Moreover, including the substrate within the macrocycle cavity appears essential for its catalytic action (Fig. 2).

Aniline is characterized by a log P_{ow} value of 0.9 and demonstrates a water solubility of 35 g L^{-1} at 20 °C, according to ECHA. The interaction between aniline and carboxylato-prism[6]arene **PrS[6]**$^{COO-}$ was determined using 1D NMR titration experiments in D_2O, and calorimetric investigations (*vide infra*). During these ^{1}H NMR titrations, the concentration of aniline was held constant while the ratio of **PrS[6]**$^{COO-}$ to aniline was gradually increased. This experiment was performed in a buffered D_2O solution (pH = 7.6). The interaction between **PrS[6]**$^{COO-}$ and aniline **2a** exhibits a fast in/out exchange rate within the NMR timescale. The signals from the guest molecules are shifted upfield due to the magnetic shielding effect of the aromatic cavity of **PrS[6]**$^{COO-}$ (Fig. 2). The association constant for forming the **2a@PrS[6]**$^{COO-}$ complex, as illustrated in the equilibrium in Fig. 2, was determined by fitting the NMR titration[35] data and through isothermal titration calorimetry (see SI). The complexes formed between **PrS[6]**$^{COO-}$ and aniline **2a** exhibit an affinity constant of 90 M^{-1}.

Based on these results, a series of experiments was conducted to investigate the impact of various reaction conditions on process efficiency. Initially, we evaluated the effect of the amount of macrocycle used. Keeping the reaction time constant, the reaction proceeded successfully even when the amount of **PrS[6]**$^{COO-}$ was reduced to 0.15 equivalents (Table 1, entries 4–6). However, further decreasing the amount to 0.05 equivalents resulted in a notable decline in reaction efficiency (Table 1, entry 7). Subsequently, we investigated the impacts of varying reaction times and temperatures while maintaining 0.15 equivalents of **PrS[6]**$^{COO-}$. Reducing the reaction time from 2 hours to 1 hour resulted in a moderate decrease in yield (Table 1, entry 9), whereas extending the reaction time to 4 hours (Table 1, entry 8) did not significantly impact the overall efficiency of the reaction. Lowering the reaction temperature from 60 °C to 25 °C decreased the reaction rate (Table 1, *cf.* entries 6 and 11), requiring a longer reaction time (Table 1, entry 12) to achieve comparable yields. Control experiments highlighted the critical role of H_2O_2 concentration. Reducing the amount of H_2O_2 by half (Table 1, entry 13) while keeping the total reaction volume constant at 2 mL by adding a phosphate buffer (pH 7.6) at a reaction temperature of 60 °C for two hours still resulted in a satisfactory yield of 71% nitrobenzene using only 50% of the catalyst. A comparison of entries 4 and 13 reveals that the aniline **2a** oxidation conversion rate is unaffected by the addition of 1 mL of phosphate buffer or a lower amount of H_2O_2 under these reaction conditions.

However, further H_2O_2 reduction significantly decreased the yield, even with extended reaction times (Table 1, entries 14–16). Simultaneously reducing both catalyst loading and H_2O_2 concentration resulted in a dramatic drop in reaction efficiency (Table 1, entry 17).

This prism[6]arene/H_2O_2/H_2O mixture can be reutilized in subsequent oxidation reactions by adding aniline **2a**. Notably, this procedure retains the catalyst's high activity level across five consecutive cycles (see SI).

With these results in hand, we further assessed the general applicability of this procedure (conditions [a] in Table 2) for a range of structurally diverse aniline derivatives (**2b–q**), with the findings summarized in Table 2. The reactivity varied based on the specific aniline employed; however, nitro derivatives were obtained as the sole products in all cases, with no side oxidation products detected in the presence of the prism[6]arene catalyst.

The reaction demonstrated compatibility with electron-donating and electron-withdrawing groups, enabling the synthesis of a broad range of substituted nitroarenes. Anilines **2b–f**, bearing alkyl groups at various positions on the aromatic ring (Table 2, entries 2–6), were smoothly converted into their corresponding nitro compounds with reasonable conversion rates. Moreover, nitro-xylene derivatives, important intermediates in various applications, were successfully obtained from the corresponding anilines *via* this method.

Table 2 Scope of the oxidation of various anilines to nitro derivatives in the presence of carboxylato-prism[6]arene **PrS[6]**$^{COO-}$ [a]

Entry	Substrate	Yield[b] (%)
1	**2a**	74
2	**2b**	80
3	**2c**	75
4	**2d**	76
5	**2e**	75
6	**2f**	85
7	**2g**	10
8	**2h**	65
9	**2i**	33
10	**2j**	75
11	**2k**	10
12	**2l**	15
13	**2m**	50
14	**2n**	13
15	**2o**	10
16	**2p**	—[c]
17	**2q**	—

[a] Conditions unless otherwise noted: **2** (0.1 mmol), **PrS[6]**$^{COO-}$ (015 equiv.), H_2O_2 (2 mL, 50% (w/w)), 60 °C, 2 h. [b] Yields were determined by ^{1}H NMR analysis of the crude reaction mixture, employing 1,1,2-trichloroethane as the internal standard. [c] The reaction mixture resulted in a complex mixture of products.

Notably, 4-isopropylaniline **2f** demonstrated a higher conversion (85%) compared to 2-isopropylaniline **2g** (10%) in producing the corresponding nitro product (Table 2, entries 6 *vs.* 7). The differing reactivities of derivatives **2f** (85%) and **2g** (10%) can be attributed to steric factors. Specifically, the bulky isopropyl group, positioned *ortho* to the NH_2 group in **2g**, depresses its reactivity, significantly reducing the oxidation yield compared to the *para*-substituted **2f**.

It is interesting to note that the conversion to the nitro derivative **3g** increases to 30% when **2g** is oxidized in the presence of an equivalent of **PrS[6]**$^{COO-}$ at 60 °C for 2 hours (Table 3, entry 1), or to 40% when oxidized at 25 °C for 24 hours (Table 3, entry 2).

An electron-donating group, such as methoxy, in the *ortho* and *para* positions of compounds **2h** and **2j**, respectively, leads to yields of 65% and 75% (Table 2, entries 8 and 10). However, when the methoxy group is in the *meta* position in compound **2i**, the oxidation yield markedly declines to 33% (Table 2, entry 9). In this case, it is also possible to significantly increase the conversion to the nitro derivative **3i** (73%) by increasing the amount of **PrS[6]**$^{COO-}$ to 1 equiv. and conducting the oxidation at room temperature for a long time (15 hours, Table 3, entry 3). Similarly, the presence of an electron-withdrawing group, such as NO_2, in the *para* position relative to the NH_2 group in the **2k** (Table 2, entry 11, 0.15 equiv. of **PrS[6]**$^{COO-}$, 60 °C, 2 h) derivative results in a dramatic reduction in the oxidation yield (10%). Fortunately, derivative **2k** can be oxidized with a conversion of 63% by increasing the amount of **PrS[6]**$^{COO-}$ to 0.5 equivalents and conducting the reaction at 60 °C for 4 hours (Table 3, entry 4).

The electronic effects of halogens in the *para*/*ortho* position are notably evident (Table 2, entries 12–14). The derivative **2m** (entry 13), which contains a chlorine atom at the *para* position, is oxidized with a moderate yield of 50% by performing the oxidation in the presence of 0.15 equivalents of **PrS[6]**$^{COO-}$ at 60 °C for 2 hours. The conversion to **3m** was increased to 70% by conducting the oxidation of **2m** in the presence of 1.0 equivalent of prismarene for 15 hours at 25 °C (Table 3, entry 6). In addition, the presence of a bromine atom in the derivative **2l** drastically reduces the oxidation yield to 15% using 0.15 equiv. of **PrS[6]**$^{COO-}$ at 60 °C for 2 hours (Table 2, entry 12). The conversion to **3l** is impressively increased to 60% by performing the oxidation of **2l** at 60 °C for 2 hours in the presence of 0.30 equivalents of **PrS[6]**$^{COO-}$ (Table 3, entry 5).

Derivative **2n**, bearing fluorine atoms in the *ortho* positions, was oxidized in low yield in the presence of 0.15 equivalents of **PrS[6]**$^{COO-}$ at 60 °C for 2 hours (Table 2, entry 14). The conversion rate increased to 45% when 1.0 equivalent of prismarene was used at 60 °C for 3 hours (Table 3, entry 7). Finally, derivative **2o**, which has electron-withdrawing groups in the *meta* (NO_2) and *para* (Cl) positions relative to the NH_2 group, was oxidized with very low conversion in the presence of 0.15 equivalents of **PrS[6]**$^{COO-}$ at 60 °C for 2 hours (Table 2, entry 15). Interestingly, the conversion rate was increased to 40% by performing the reaction in the presence of 1.0 equivalent of **PrS[6]**$^{COO-}$ at 25 °C for 15 hours (Table 3, entry 8). Unfortunately, the derivatives 1-naphthylamine **2p** and 2-aminoanthracene **2q** failed to produce the desired nitro products when treated with 0.15 or 1.0 equivalents of **PrS[6]**$^{COO-}$ at 60 °C for 2 hours. This lack of reactivity is likely due to the poor water solubility of these derivatives and the larger size of anilines **2p** and **2q**, which probably restricts their access to the cavity of **PrS[6]**$^{COO-}$. Both factors hinder the oxidation process.

The results in Tables 2 and 3 emphasize that the conversion rates of H_2O_2/**PrS[6]**$^{COO-}$ mediated oxidation of aniline derivatives **2a–q** are strongly influenced by the steric and electronic effects of the substrates. The presence of electron-withdrawing groups in the *para* position relative to the oxidizable NH_2 group significantly decreases the substrate reactivity. This effect is similarly observed for substituents in the *ortho* position adjacent to the reactive NH_2 group. Furthermore, derivatives that do not fit within the cavity, such as **2p** and **2q**, exhibit no signs of oxidation to form the target product **3**.

Table 3 Improving Reaction Conversion through Customization of Reaction Parameters

Entry[a]	Substrate	**PrS[6]**$^{COO-}$ (equiv.)	T (°C)/*t* (h)	Yield[b] (%)
1	**2g**	1.0	60/2	30
2	**2g**	1.0	25/24	40
3	**2i**	1.0	25/15	73
4	**2k**	0.50	60/4	63
5	**2l**	0.30	60/2	60
6	**2m**	1.0	25/15	70
7	**2n**	1.0	60/3	45
8	**2o**	1.0	25/15	40
9	**2p**	1.0	60/2	—[c]
10	**2q**	1.0	60/2	—

[a] Reactions were conducted on a 0.1 mmol scale of derivatives **2** in 2 mL of 50% (w/w) H_2O_2. [b] Yield determined by ^{1}H NMR analysis of the crude reaction mixture using 1,1,2-trichloroethane as the internal standard. [c] The reaction mixture contained a complex mixture of products.

Calorimetric investigations

ITC calorimetry provides a unique perspective for enhancing the design of adaptable synthetic macrocyclic hosts and gaining essential insights into the catalytic frameworks that exploit host–guest interactions to promote scalable and sustainable (bio)catalysis.[37]

Calorimetric measurements assessed the thermodynamic parameters influencing the recognition processes occurring in aqueous solution between the macrocyclic **PrS[6]**$^{COO-}$ receptor and selected aromatic amines. These molecules were chosen as model compounds to examine how the position, number, type of substituents, and molecular size may influence host–guest complex formation.

Representative calorimetric titration for the formation of the **2a@PrS[6]**$^{COO-}$ complex is shown in Fig. 3, whereas titrations for all the investigated systems are illustrated in Fig. S50–S56. The analysis of the calorimetry data indicated that the **PrS[6]**$^{COO-}$ host interacts with the aromatic substrates, forming only 1 : 1 complex species as its cavity cannot accommodate

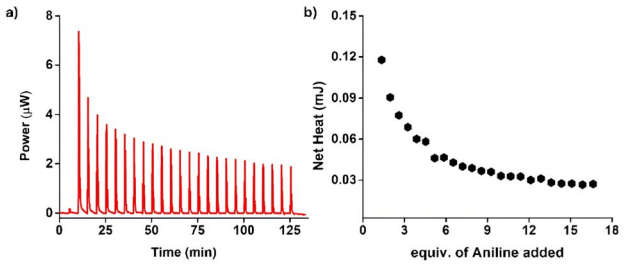

Fig. 3 (a) ITC titration of PrS[6]$^{COO-}$ (0.92 mM) with aniline **2a** (up to 16.6 equiv.) at 25 °C and pH 7.6; (b) integrated net heat curve.

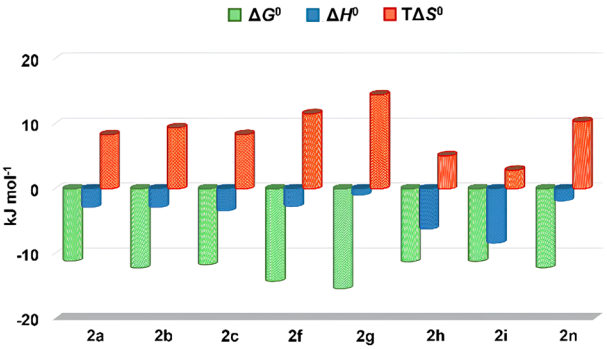

Fig. 4 Thermodynamic parameters for the host–guest complex formation in aqueous solution at 25 °C and pH 7.6.

multiple guest molecules simultaneously. The association constants range from 90 to 500 M^{-1} (Table 4), depending on the structural properties of the guests bearing different numbers and kinds of functional groups in various positions of the aromatic ring. The binding affinities for these amino substrates are smaller than those previously reported for differently charged and shaped cationic guests, expectedly due to the lack of electrostatic and dipolar interactions, which favored the stability of the host–guest complexes in the latter case.[32]

ITC measurements further provided a complete thermodynamic profile for the complexation of aromatic amines within the cavity of **PrS[6]$^{COO-}$** for a sharper elucidation of the mechanisms that regulate the binding processes in solution (Table 4 and Fig. 4). The binding of aniline **2a** occurs through an entropically favored and driven process that may be attributed to the disruption of the hydrogen bond network surrounding both the host and guest molecules, which undergo desolvation to form the complex species (hydrophobic effect, *vide infra* and Fig. 5).[38,39] The structural rearrangement of the macrocycle receptor, which can suitably tilt its cavity walls to better accommodate the guest, further contributes to the positive entropic term. Enthalpy also favors the complexation process, albeit to a lesser extent; this observation is consistent with the release of high-energy water molecules from the prismarene cavity (Fig. 5), thus contributing to the thermodynamic stability of the inclusion complex.[40] **PrS[6]$^{COO-}$** exhibits a slightly increased affinity towards guests bearing methyl (**2b** and **2c**) or fluorine (**2n**) substituents. The complex formation is again entropically driven and accompanied by a slightly favorable enthalpy contribution. The magnitude of both terms is comparable to that obtained for the aniline complex, suggesting that introducing such substituents on the aromatic ring does not affect the mechanisms of recognition.

Complexes incorporating the bulkier isopropylanilines **2f** and **2g** exhibit enhanced thermodynamic stability, likely due to their optimal accommodation within the host cavity. Although binding remains entropically driven, it is further favored by a modest enthalpic contribution.

The entropy gain observed for these guests is the highest among those investigated (Fig. 4). This pronounced entropic effect can be attributed to a significant desolvation

Table 4 log K values and binding parameters[a] for the host–guest complexes formed by PrS[6]$^{COO-}$ with aromatic amines in aqueous solution at 25 °C and pH 7.6

Substrate	log K	ΔH^0 (kJ mol^{-1})	ΔS^0 (J K^{-1} mol^{-1})
2a	1.95 (5)	−2.83 (3)	28 (1)
2b	2.14 (6)	−2.83 (3)	32 (2)
2c	2.05 (7)	−3.36 (4)	28 (2)
2f	2.50 (1)	−2.71 (5)	39 (2)
2g	2.70 (1)	−0.93 (6)	50 (3)
2h	1.97 (7)	−6.19 (4)	17 (2)
2i	1.96 (6)	−8.36 (3)	10 (2)
2n	2.13 (9)	−1.82 (5)	35 (2)

[a] σ in parentheses.

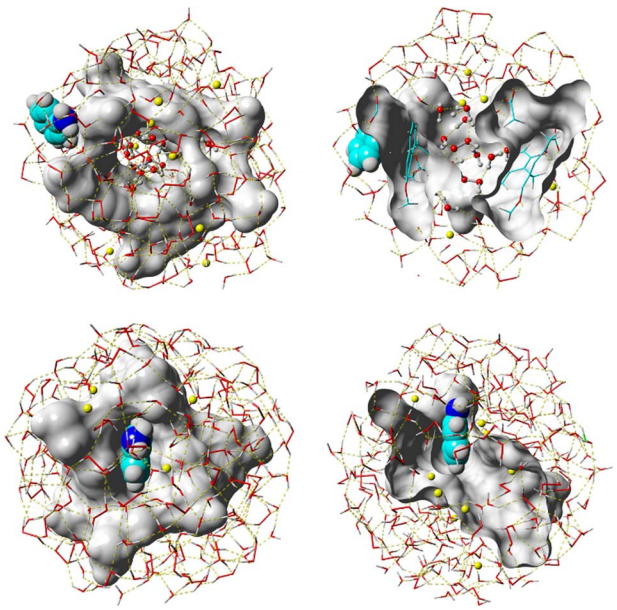

Fig. 5 Top (up left) and side section (up right) views of the **2a** + PrS[6]^{COONa} inside the spherical nanoreactor; top (bottom left) and side section (bottom right) views of the **2a** + PrS[6]^{COONa} inside the spherical nanoreactor. Compound **2a** and Na^+ ions are represented as balls (in the upper right, also H_2O and H_2O_2 molecules within the cavity), H_2O and H_2O_2 molecules as stick lines, and PrS[6]^{COONa} is rendered as a molecular surface. Dashed lines represent hydrogen bonds.

phenomenon, whereby more water molecules are displaced from the inner cavity to accommodate these sterically demanding guests. Overall, the hydrophobic effect appears to be the principal driver behind forming the series's most stable host–guest complexes. Moreover, it is plausible that the *ortho*-substituted, bulkier guest **2g** induces a more substantial structural rearrangement of the host scaffold than **2f**, resulting in an even more favorable entropy gain and higher binding affinity.

Though electron-donating groups in anisidines (**2h** and **2i**) do not alter the strength of the interaction with **PrS[6]**$^{COO-}$ compared to the unsubstituted substrate, a completely different thermodynamic signature is observed. The molecular recognition of both guests is primarily enthalpy-driven, with the entropy term still providing a favorable contribution. The enthalpy gain is consistent with the establishment of water-mediated hydrogen-bond interactions with the carboxylato prismarene, as already described for including hydrogen-bond acceptor guests within the analogous five-membered macrocycle.[34] As in the case of substrates having isopropyl substituents, the more considerable entropy gain is observed for the complexation of the guest with the methoxy moiety closer to the amino group (**2h**). The inclusion of some of the guests examined in the present work into various macrocyclic cavities has been reported in the literature, but thermodynamic parameters have rarely been discussed. Moreover, the quite different experimental conditions employed make any direct comparison difficult.[41–43]

For example, the inclusion of protonated aniline derivatives within α,α′,δ,δ′-tetramethyl-cucurbit[6]uril or cucurbit[7]uril was found to be driven by a significant favorable enthalpic contribution ascribed to ion–dipole interactions between the positively charged guests and the carbonyl oxygens on the host rim as well as interactions between the aromatic ring of the guests and the inner wall of the macrocycle. These attractive forces resulted in higher stability constants, consistent with our previous observations on encapsulating charged guests into carboxylato prismarenes.[28,29] The inclusion of *o*-anisidine within a β-cyclodextrin cavity is likewise driven by enthalpy, as observed here for **PrS[6]**$^{COO-}$; in both cases, the recognition process is guided by the formation of water-mediated hydrogen bonds resulting in comparable binding affinity (Fig. 5).

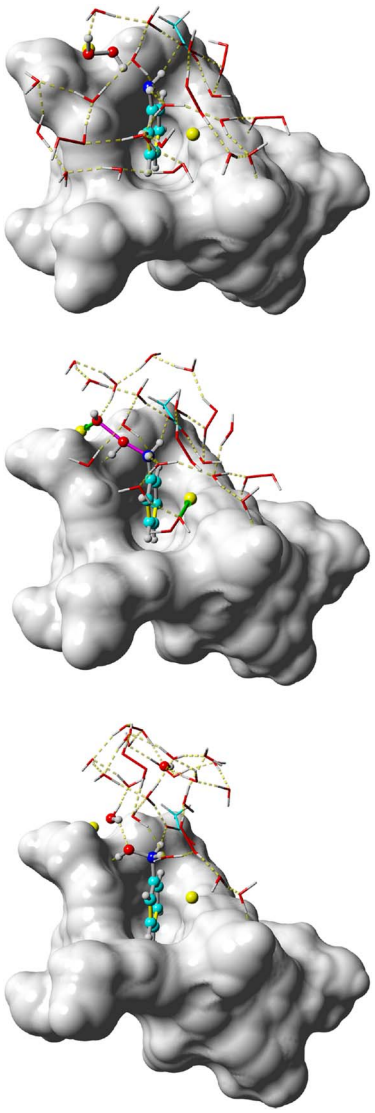

Fig. 6 Detail of **2a**@PrS[6]^{COONa} (top), **2a**@PrS[6]^{COONa}-TS (middle) and **2a**@PrS[6]^{COONa}-P (down). Compound **2a**, one interacting H_2O_2 molecule, and Na^+ ions are represented as balls, H_2O and H_2O_2 molecules as stick lines, and PrS[6]$^{COO-}$ is rendered as a molecular surface. Dashed lines represent hydrogen bonds.

In Silico calculations

To rationalize the experimental data and provide robust support for a plausible reaction mechanism, we conducted a comprehensive computational study (Fig. 5–7 and Scheme 2), using the oxidation of aniline as a reference reaction. This approach enabled us to investigate the key interactions and energetic profiles that govern the process.

The experimental observations strongly suggest a mechanistic pathway in which, in the first step of the reaction, the aniline-NH_2 group serves as a nucleophile, actively attacking the peroxy bond's oxygen atom (Fig. 6 and 7 and Scheme 2).[28,29] This nucleophilic interaction is likely facilitated by the activation of hydrogen peroxide through a well-organized network of hydrogen bonds. These bonds are mediated by water molecules strategically positioned and probably anchored to carboxylate groups, thereby enhancing the overall reactivity of the system (Fig. 6 and 7 and Scheme 2).[34] Our research group has previously proposed this model to explain the aqueous-phase recognition of hydrophilic amines by carboxylato-prismarenes.[34]

Given the inherent complexity of the system, where both solvent effects and the concentration of the oxidant must be carefully considered, we employed the semiempirical GFN2-xTB extended tight binding[44] computational approach to simulate the reaction environment, focusing on the initial stage of the reaction. Specifically, we investigated the interaction of compound **2a** with H_2O_2 within a confined spherical nanoreactor with a diameter of 28 Bohr. This model system was designed to mimic experimental conditions closely, incorporating a molecule of compound **2a** and a molecule of the

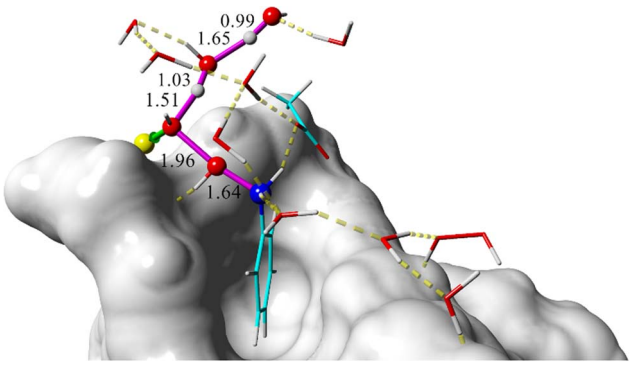

Fig. 7 Expanded detail of the **2a@PrS[6]**^{COONa}-TS. Magenta lines represent TS bonds, dashed yellow lines hydrogen bonds, and green line dative bond (oxygen lone pair interactions with Na^+ empty orbital). Distances are in Å.

substrate **PrS[6]**^{COONa}, both immersed in an aqueous hydrogen peroxide mixture. The nanoreactor (NR) contained 173 water molecules and 90 hydrogen peroxide molecules, corresponding to the 50% (w/w) H_2O_2 solution used in the experimental setup (see SI for details).

By leveraging this computational framework, we aimed to capture the reaction's dynamic behavior more realistically, providing critical insights into the key molecular interactions that govern the oxidation process.

To obtain a clear and meaningful assessment of the importance and effect of substrate complexation within the prismarene cavity during oxidation, we constructed two distinct systems (Fig. 5): one in which compound **2a** remained outside the cavity (NR_{out}) and another in which it was encapsulated within (NR_{in}). This comparative approach aimed to elucidate the potential influence of host–guest interactions on the reaction mechanism and energetics.

Both systems underwent a conformational search using the low-energy diversity-enhanced variant of CREST (LEDE-CREST),[45] an advanced adaptation of the CREST iMTD algorithm designed explicitly for noncovalent clusters of flexible molecules.[46] The most stable conformers identified through this procedure were subsequently selected for further computational studies.

Before conducting a detailed investigation of the reaction pathway, beginning with the proposed nucleophilic attack, we employed a nanoreactor-based approach for chemical reaction space exploration (see SI for details).[47] This simulation was designed to probe the oxidation reaction, capture possible mechanistic pathways, and identify intermediate products. However, due to the complexity of the system and the large number of molecules involved, this method primarily served to validate our hypothesis regarding the initiation of the reaction. The results confirmed that the first step proceeds *via* the nucleophilic addition mechanism postulated in our model, yielding phenylhydroxylamine as the sole observed product.

Encouraged by this finding, we proceeded with an in-depth study of the nucleophilic addition mechanism in both systems, comparing the energetic landscapes associated with

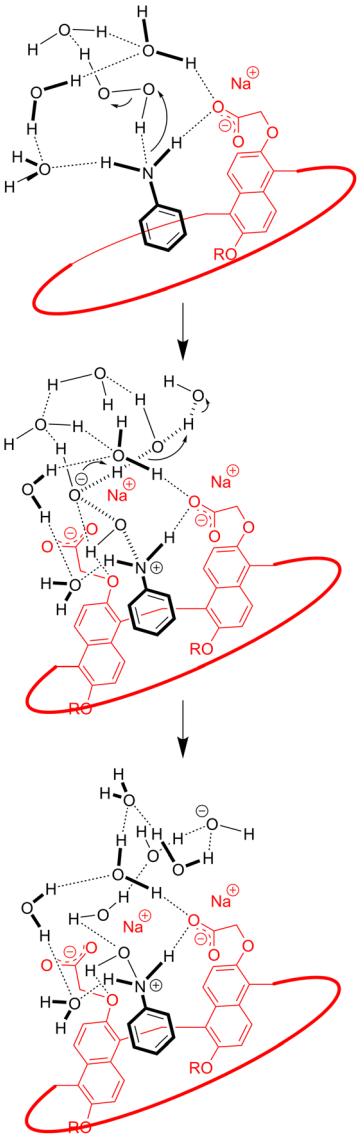

Scheme 2 Proposed mechanism of the first stage of the reaction promoted by prismarene, based on *in silico* investigation. Dotted lines represent hydrogen bonds, whereas transverse dashed lines represent bonds that form and break in the TS.

the first oxidation step inside and outside the prismarene cavity. The computed energetic results are summarized in Tables 5 and S2, while Fig. 5 illustrates the top and side views of the two studied systems. In Fig. 6, the optimized 3D geometries of the system, in which compound **2a** is confined within the prismarene cavity, are reported. Additionally, Fig. 7 provides a detailed visualization of the key interactions occurring at the **2a@PrS[6]**^{COONa} transition state, offering deeper insight into the structural and electronic factors governing the reaction. Visual analysis of Fig. 5 provides key insights into the structural differences between the two studied systems.

In the NRout system, compound **2a** is positioned near the naphthalene components of prismarene (Fig. 5, top left), leading to a contraction of the prismarene framework as it

Table 5 Differences in enthalpy, Gibbs free energy, and entropy values for the **2a** + **PrS[6]**^{COONa} and **2a@PrS[6]**^{COONa} systems in the spherical nanoreactor immersed in the 50% (w/w) H_2O_2 aqueous solution

Nanoreactor systems NR_{out} and NR_{in}	$\Delta\Delta H^a$	$\Delta\Delta G^a$	$T\Delta\Delta S^a$
2a + **PrS[6]**^{COONa}	0	0	0
2a + **PrS[6]**^{COONa}-TS	89.04^b	106.40^b	−17.36^b
2a + **PrS[6]**^{COONa}-P	−24.34^b	−8.28^b	−16.15^b
2a@PrS[6]^{COONa}	−3.56^b	−11.38^b	7.82^b
2a@PrS[6]^{COONa}-TS	56.77^c	71.46^c	−14.69^c
2a@PrS[6]^{COONa}-P	−21.69^c	−9.54^c	−2.90^c

^{a} All values are in kJ mol^{-1}. ^{b} Relative to **2a** + **PrS[6]**^{COONa} system. ^{c} Relative to **2a@PrS[6]**^{COONa} system.

attempts to minimize the volume of its internal hydrophobic cavity. Despite this structural adjustment, several solvent molecules, specifically, 11 water molecules and one hydrogen peroxide molecule, remain trapped within the cavity (Fig. 5, top right). The proposed mechanism of the first stage of the reaction promoted by prismarene, based on *in silico* investigation, is reported in Scheme 2.

Conversely, in the NR_{in} system, the prismarene cavity undergoes a conformational adaptation to encapsulate compound **2a**, effectively reshaping itself around the guest molecule. This structural reorganization results in the complete expulsion of solvent molecules from the hydrophobic pocket (Fig. 5, bottom). Additionally, the aniline group of compound **2a** is anchored at the upper edge of prismarene, stabilized by two key hydrogen bonds: one involving an oxygen atom from a carboxylate group and the other mediated by a water molecule. The latter is further stabilized through an extensive hydrogen-bonding network with adjacent solvent molecules (Fig. 6, top).

The energy data presented in Table 5 for both systems (**2a** + **PrS[6]**^{COONa} and **2a@PrS[6]**^{COONa}) align closely with experimentally obtained calorimetric values, confirming the reliability of the computational model. The **2a@PrS[6]**^{COONa} system is energetically favored due to both enthalpic and entropic contributions.

A comparative thermodynamic analysis reveals significant differences in enthalpy, Gibbs free energy, and entropy values between the **2a** + **PrS[6]**^{COONa} and the encapsulated **2a@PrS[6]**^{COONa} systems within a spherical nanoreactor immersed in a 50% (w/w) H_2O_2 aqueous solution. These differences underscore how the spatial confinement provided by the nanoreactor alters molecular interactions and reaction energetics. In particular, the encapsulated system exhibits distinct enthalpic contributions, reflecting variations in non-covalent interactions and bond stabilization. The observed entropy differences, on the other hand, point to altered solvation dynamics and ordering effects under highly oxidizing conditions, providing key insights into how nanoconfinement modulates reactivity and stability in such complex chemical systems.

Interestingly, the thermodynamic differences in the oxidizing conditions are similar to those observed in calorimetric studies conducted in water alone. This similarity suggests that, despite the oxidizing conditions of the H_2O_2 medium, the underlying molecular interactions and nanoconfinement effects governing the host–guest dynamics remain unchanged. Consequently, the trends in stability and binding energetics appear to be primarily driven by intrinsic host–guest interactions rather than the specific solvent environment. From the analysis of the values reported in Table 5, it is evident that while the nucleophilic substitution reaction can proceed in both systems, the activation free energy for the transition state **2a@PrS[6]**^{COONa}-TS is 34.94 kJ mol^{-1} lower than that of the corresponding **2a** + **PrS[6]**^{COONa}-TS. This energy difference suggests that the encapsulated system (NR_{in}) significantly facilitates the reaction, whereas the non-encapsulated system (NR_{out}) is penalized enthalpically and entropically. To understand the origin of this lower activation energy, we analyzed the bond interactions present in the optimized transition state (TS) geometry obtained from our computational calculations for the NR_{in} system (Fig. 6, middle, and Fig. 7). As shown in Fig. 6, the highly coordinated nature of bond formation and cleavage is clearly visible, along with the stabilizing role of the extended hydrogen bond network. A detailed examination of the TS reveals the following key mechanistic insights:

- The N–O bond formation occurs at a distance of 1.64 Å, while the O–O bond undergoes cleavage at 1.96 Å.
- The departing hydroxyl ion from the peroxide is stabilized by one of the sodium cations, which is itself coordinated with a carboxylate oxygen atom.
- Simultaneously, the hydroxyl ion begins to extract a hydrogen atom from an adjacent water molecule, initiating a proton transfer cascade.
- This water molecule, in turn, begins to deprotonate another nearby water molecule, a process that is fully completed upon the formation of the final product **PrS[6]**^{COONa}-P.
- Additionally, the hydrogen atom attached to the oxygen forming the hydroxylamine bond is stabilized *via* a hydrogen bond with a phenolic-type oxygen of the prismarene.
- Finally, the two hydrogen atoms of the aniline nitrogen remain anchored to the system through the same hydrogen bonds observed in the initial structure, maintaining their interactions throughout the reaction.

These findings highlight the crucial role of the prismarene cavity in lowering the activation barrier by providing an optimal reaction environment, stabilizing key intermediates, and facilitating proton transfer through an extended hydrogen bond network. The reaction scheme is ultimately completed with the formation of phenylhydroxylamine, which remains securely anchored within the hydrophobic cavity of the prismarene. This encapsulation likely stabilizes the product, preventing its premature diffusion into the surrounding solvent environment. Meanwhile, the released hydroxide ion becomes entrapped within the extensive hydrogen bond network formed by the surrounding solvent molecules (Fig. 6, bottom). This stabilization by hydrogen bonding likely mitigates any destabilizing effects that could arise from the presence of a free hydroxide ion, further supporting the role of the prismarene cavity in orchestrating the reaction.

Conclusions

The carboxylato-prism[6]arene can catalyze the oxidation of aromatic amines in water using a green oxidant such as hydrogen peroxide. The reaction occurs in the presence of aniline derivatives bearing aliphatic groups in various *ortho*, *meta*, and *para* positions, as well as electron-donating and electron-accepting substituents. The oxidized product can be extracted using ethyl acetate, while the prism[6]arene/H_2O_2/H_2O mixture can be reused by adding aniline. The system maintains its efficiency for up to five consecutive cycles. NMR studies, alongside an in-depth calorimetric investigation, confirm that the formation of the supramolecular complex in water between the aniline derivatives and the prismarene is crucial for catalysis. The formation of the endo-cavity complex is primarily driven by entropic factors, attributable to host and guest desolvation, including the expulsion of frustrated water from the deep prismarene cavity.

In silico calculations provide insights into the key driving forces governing the encapsulation of aromatic amines within the prismarene cavity. The computational study complements our experimental findings and refines our understanding of the role of hydrogen bonding and solvent effects in facilitating the oxidation reaction. The computational results strongly suggest that the adopted model effectively replicates the experimental system, reinforcing the accuracy of our approach in capturing key molecular interactions and thermodynamic parameters.

By comparing the encapsulated and non-encapsulated systems, we demonstrate that the prismarene cavity significantly enhances the oxidation process by reducing the activation energy by 34.94 kJ mol^{-1} for the transition state within the cavity. The reaction is facilitated through hydrophobic interactions, stabilization *via* hydrogen bonding, and an efficient proton transfer network, as evidenced by the structural analysis of the transition state. These findings validate the computational framework utilized and highlight the potential of host–guest chemistry in modulating reaction mechanisms.

Ultimately, this study offers fundamental insights into the initial stages of this oxidation process, providing a valuable foundation for future research on confined reaction environments.

Author contributions

M. D. R., C. G., A. R. and C. S. conceived and supervised the research; R. D. R, G. C. executed the experiments and analyzed the experimental data; C. S. and G. D. G. S. performed calorimetric investigations and rationalized the experimental results; A. R. carried out the computational studies and analyzed the results; P.N. and C. T. were responsible for data curation; R. D. R prepared the SI and performed the characterization of all compounds and NMR studies; M. D. R., C. G., A. R. and C. S. wrote the manuscript and performed manuscript edits and revisions. All authors participated in discussions and approved the final manuscript.

Conflicts of interest

There are no conflicts to declare.

Data availability

The data supporting this article have been included as part of the SI. Supplementary information: Experimental procedures, NMR spectra, ITC and computational details. See DOI: **https://doi.org/10.1039/d5sc03155a**.

Acknowledgements

This work has been partially supported by MUR in the framework of PNRR, Mission 4, Component 2, Investment 1.5, under the project SAMOTHRACE (ECS00000022), PRIN_PNRR 2022: prismarene-based chemosensors for monitoring organic water contaminants (PRISMASENS) (PRIN_PNRR P2022XHLTX), CUP D53D23017250001. The authors C. T., A. R., C. G., M.D.R. are associated to the "Consorzio Interuniversitario Nazionale di ricerca in Metodologie e Processi Innovativi di Sintesi" (CINMPIS).

Notes and references

1 P. D. Boyer, *Annu. Rev. Biochem.*, 1997, **66**, 717–749.
2 L. Michaelis, M. L. Menten, K. A. Johnson and R. S. Goody, *Biochemistry*, 2011, **50**, 8264–8269.
3 A. J. Kirby and F. Hollfelder, in *From Enzyme Models to Model Enzymes*, ed. A. J. Kirby and F. Hollfelder, Royal Society of Chemistry, Cambridge, 2009.
4 R. Breslow, *Science*, 1982, **218**, 532–537.
5 M. Raynal, P. Ballester, A. Vidal-Ferran and P. W. N. M. van Leeuwen, *Chem. Soc. Rev.*, 2014, **43**, 1734–1787.
6 B. W. Purse and J. Rebek Jr., *Proc. Natl. Acad. Sci. U. S. A.*, 2005, **102**, 10777–10782.
7 M. De Rosa, P. La Manna, C. Talotta, A. Soriente, C. Gaeta and P. Neri, *Front. Chem.*, 2018, **6**, 84.
8 F. Ortega-Caballero, C. Rousseau, B. Christensen, T. E. Petersen and M. Bols, *J. Am. Chem. Soc.*, 2005, **127**, 3238–3239.
9 C. A. Vezzoni, A. Casnati, S. Orlanducci, F. Sansone and R. Salvio, *ChemCatChem*, 2024, **16**, e202301477.
10 B. Tang, J. Zhao, J.-F. Xu and X. Zhang, *Chem.–Eur. J*, 2020, **26**, 15446–15460.
11 M. De Rosa, S. Gambaro, A. Soriente, P. Della Sala, V. Iuliano, C. Talotta, C. Gaeta, A. Rescifina and P. Neri, *Chem. Sci.*, 2022, **13**, 8618–8625.
12 K. Wang, J. H. Jordan, K. Velmurugan, X. Tian, M. Zuo, X.-Y. Hu and L. Wang, *Angew. Chem., Int. Ed.*, 2021, **60**, 9205–9214.
13 C. Gaeta, P. La Manna, M. De Rosa, A. Soriente, C. Talotta and P. Neri, *ChemCatChem*, 2021, **13**, 1638–1658.
14 Q. Zhang, L. Catti and K. Tiefenbacher, *Acc. Chem. Res.*, 2018, **51**, 2107–2114.
15 G. Borsato, J. Rebek Jr. and A. Scarso, in *Selective Nanocatalysts and Nanoscience*, ed. A. Zecchina, S. Bordiga

and E. E. Groppo, Wiley-VCH, Weinheim, Germany, 2011, pp. 105–168.
16 S. H. A. M. Leenders, R. Gramage-Doria, B. de Bruin and J. N. H. Reek, *Chem. Soc. Rev.*, 2015, **44**, 433–448.
17 C. M. Hong, R. G. Bergman, K. N. Raymond and F. D. Toste, *Acc. Chem. Res.*, 2018, **51**, 2447–2455.
18 N. Ono, in *The Nitro Group in Organic Synthesis*, Wiley-VCH, Weinheim, 2001.
19 H. Zollinger, *Color Chemistry*, Wiley-VCH, New York, 1987, p. 161.
20 K. Nepali, H.-Y. Lee and J.-P. Liou, *J. Med. Chem.*, 2019, **62**, 2851–2893.
21 R. F. Fan, Y. Yao, L. Cai, L. Cheng, J. M. Tour and A. J. Bard, *J. Am. Chem. Soc.*, 2004, **126**, 4035–4042.
22 (*a*) H. Surburg, in *J. Panten Common Fragrance and Flavor Materials. Preparation, properties and uses*, 6th Wiley-VCH Verlag GmbH & Co. KGaA, Weinheim, 2016; (*b*) C. Sommer, in *Synthetic Musk Fragrances in the Environment*, ed. G. G. Rimkus, Springer, Berlin, Heidelberg, 2004, ch. 1, pp. 1–16.
23 Y.-E. Qian, L. Zheng, H.-Y. Xiang and H. Yang, *Org. Biomol. Chem.*, 2021, **19**, 4835–4851.
24 S. Patra, I. Mosiagin, R. Giri and D. Katayev, *Synthesis*, 2022, **54**, 3432–3472.
25 E. Voutyritsa, A. Theodorou, M. G. Kokotou and C. G. Kokotos, *Green Chem.*, 2017, **19**, 1291–1298.
26 V. Daikopoulou, E. Skliri, E. D. Koutsouroubi, G. S. Armatas and I. N. Lykakis, *ChemPlusChem*, 2022, **87**, e202100413.
27 G. K. Dewkar, M. D. Nikalje, I. S. Ali, A. S. Paraskar, H. S. Jagtap and A. Sudalai, *Angew. Chem., Int. Ed.*, 2001, **40**, 405–408.
28 L. G. Marinescu, M. Mølbach, C. Rousseau and M. Bols, *J. Am. Chem. Soc.*, 2005, **127**, 17578–17579.
29 T. H. Fenger, L. G. Marinescu and M. Bols, *Org. Biomol. Chem.*, 2009, **7**, 933–940.
30 P. Della Sala, R. Del Regno, C. Talotta, A. Capobianco, N. Hickey, S. Geremia, M. De Rosa, A. Spinella, A. Soriente, P. Neri and C. Gaeta, *J. Am. Chem. Soc.*, 2020, **142**, 1752–1756.
31 P. Della Sala, R. Del Regno, V. Iuliano, A. Capobianco, C. Talotta, S. Geremia, N. Hickey, P. Neri and C. Gaeta, *Chem.–Eur. J*, 2023, **29**, e202203030.
32 R. Del Regno, G. D. G. Santonoceta, P. Della Sala, M. De Rosa, A. Soriente, C. Talotta, A. Spinella, P. Neri, C. Sgarlata and C. Gaeta, *Org. Lett.*, 2022, **24**, 2711–2715.
33 The acronym **PrS[6]**$^{COO^-}$ was previously introduced by us in ref. 32. The abbreviation PrS[6] is derived from the key letters of PriSm[6]arene, while the COO^- as a superscript highlights the presence of carboxylate substituents on the macrocycle's rim. Similar abbreviations are used for other macrocycles, such as cucurbiturils (CB[*n*]), cyclodextrins (CD), and pillar[*n*]arene (P[*n*]).
34 R. Del Regno, P. Della Sala, G. D. G. Santonoceta, P. Neri, M. De Rosa, C. Talotta, C. Sgarlata, A. De Simone and C. Gaeta, *Chem.–Eur. J*, 2024, **30**, e202401734.
35 *The association constant was calculated using the calculator Bindfit*, **http://app.supramolecular.org/bindfit/**; P. Thordarson, *Chem. Soc. Rev.*, 2011, **40**, 1305–1323; D. B. Hibbert and P. Thordarson, *Chem. Commun.*, 2016, **52**, 12792–12805.
36 Although hydrogen peroxide is acknowledged as a highly effective oxidizing agent, its ability to oxidize organic compounds is generally limited when utilized alone. Consequently, the incorporation of catalysts or additional reagents is often essential to enhance its activation. One method for activating hydrogen peroxide involves direct activation under acidic or basic conditions. To ascertain that the activation of H_2O_2 is attributable solely to the presence of carboxylato-prismarene, we conducted studies (entries 13–17) in a buffered solution at pH 7.6.
37 S. Li, Y. Xie, B. Zhang, Y. Liu, S. Xu, H. Wu, R. Du and Z.-G. Wang, *ACS Appl. Mater. Interfaces*, 2024, **16**, 45319–45327.
38 C. Sgarlata, C. Bonaccorso, F. G. Gulino, V. Zito, G. Arena and D. Sciotto, *New J. Chem.*, 2009, **33**, 991–998.
39 L. Escobar and P. Ballester, *Chem. Rev.*, 2021, **121**, 2445–2514.
40 C. Sgarlata, J. S. Mugridge, M. D. Pluth, V. Zito, G. Arena and K. N. Raymond, *Chem.–Eur. J*, 2017, **23**, 16813–16820.
41 R.-L. Lin, G.-S. Fang, W.-Q. Sun and J.-X. Liu, *Sci. Rep.*, 2016, **6**, 39057.
42 F. Wei, S.-M. Liu, G.-Z. Cheng, C.-T. Wu and Y.-Q. Feng, *Electrophoresis*, 2005, **26**, 2214–2222.
43 K. Srinivasan, J. Vaheethabanu, P. Manisankar and T. Stalin, *J. Mol. Struct.*, 2011, **987**, 214–220.
44 C. Bannwarth, S. Ehlert and S. Grimme, *J. Chem. Theory Comput.*, 2019, **15**, 1652–1671.
45 N. J. King, I. D. LeBlanc and A. Brown, *J. Comput. Chem.*, 2024, **45**, 2431–2439.
46 P. Pracht, S. Grimme, C. Bannwarth, F. Bohle, S. Ehlert, G. Feldmann, J. Gorges, M. Müller, T. Neudecker, C. Plett, S. Spicher, P. Steinbach, P. A. Wesołowski and F. Zeller, *J. Chem. Phys.*, 2024, **160**, 114110.
47 S. Grimme, *J. Chem. Theory Comput.*, 2019, **15**, 2847–2862.